Cancer Cell, Volume *34*

Supplemental Information

Enhanced Anti-lymphoma Activity of CAR19-iNKT Cells Underpinned by Dual CD19 and CD1d Targeting

Antonia Rotolo, Valentina S. Caputo, Monika Holubova, Nicoleta Baxan, Olivier Dubois, Mohammed Suhail Chaudhry, Xiaolin Xiao, Katerina Goudevenou, David S. Pitcher, Kyriaki Petevi, Carolina Kachramanoglou, Sandra Iles, Kikkeri Naresh, John Maher, and Anastasios Karadimitris

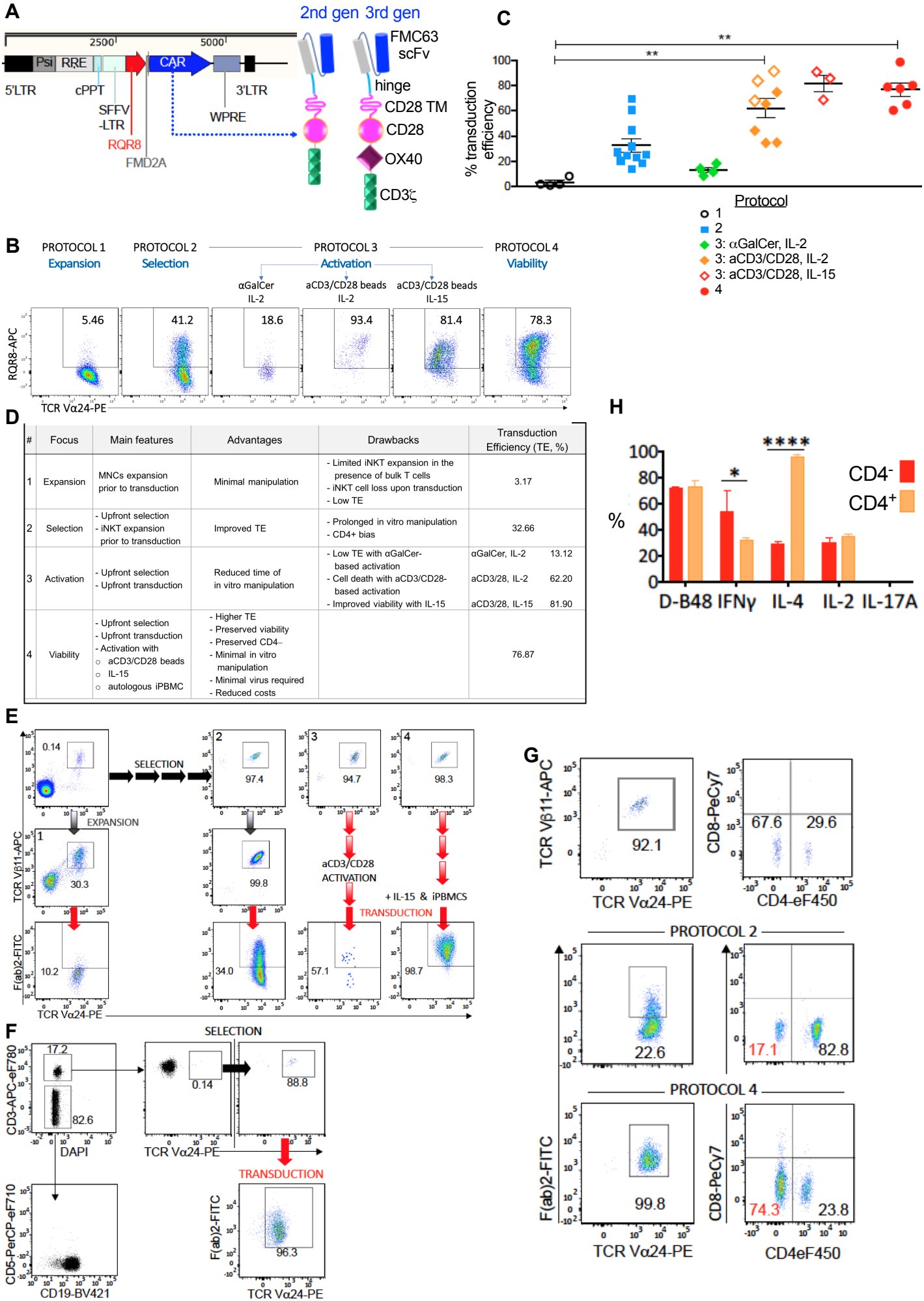

#	Focus	Main features	Advantages	Drawbacks	Transduction Efficiency (TE, %)	
1	Expansion	MNCs expansion prior to transduction	Minimal manipulation	- Limited iNKT expansion in the presence of bulk T cells - iNKT cell loss upon transduction - Low TE	3.17	
2	Selection	- Upfront selection - iNKT expansion prior to transduction	Improved TE	- Prolonged in vitro manipulation - CD4+ bias	32.66	
3	Activation	- Upfront selection - Upfront transduction	Reduced time of in vitro manipulation	- Low TE with αGalCer-based activation - Cell death with aCD3/CD28-based activation - Improved viability with IL-15	αGalCer, IL-2 aCD3/28, IL-2 aCD3/28, IL-15	13.12 62.20 81.90
4	Viability	- Upfront selection - Upfront transduction - Activation with ○ aCD3/CD28 beads ○ IL-15 ○ autologous iPBMC	- Higher TE - Preserved viability - Preserved CD4– - Minimal in vitro manipulation - Minimal virus required - Reduced costs		76.87	

Figure S1 (Related to Figure 1)

(A) Lentiviral construct and modular structure of 2nd and 3rd generation CAR19 used in this study. RQR8 is co-expressed with CAR after post-translational cleavage of the FMD2A peptide. TM: transmembrane

(B) Representative flow cytometry dot plots illustrating iNKT cell transduction efficiency according to different protocols 1-4 and the impact of IL-2 *vs* IL-15 in protocol 3.

(C) Cumulative data of B, open orange and red diamonds signify experiments performed side-by-side using same healthy donors as source of iNKT cells.

(D) Comparative summary of protocols 1-4.

(E) Representative flow-cytometry dot plots illustrating the different steps of selection, expansion and CAR transduction of iNKT cells in the 4 different protocols explored (protocols 1-4). CAR expression here is identified by anti-F(ab)2 staining.

(F) Example of generation of CAR19-iNKT cells from a patient with active lymphoma using protocol 4. CD19^{+} lymphoma cells are 82% of blood mononuclear cells.

(G) Representative example of CD4^{-} iNKT cell frequency preservation before (top dot plots) and after (middle and bottom dot plots) CAR19 transduction according to protocols 2 *vs* 4.

(H) Cumulative data showing intracellular cytokine expression by CD4^{-} and CD4^{+} CAR19-iNKT cells after C1R-CD1d cell stimulation for 4 hr. IFNγ: interferon-γ

Error bars represent SEM; *: $p<0.05$; **: $p<0.01$; ****: $p<0.0001$

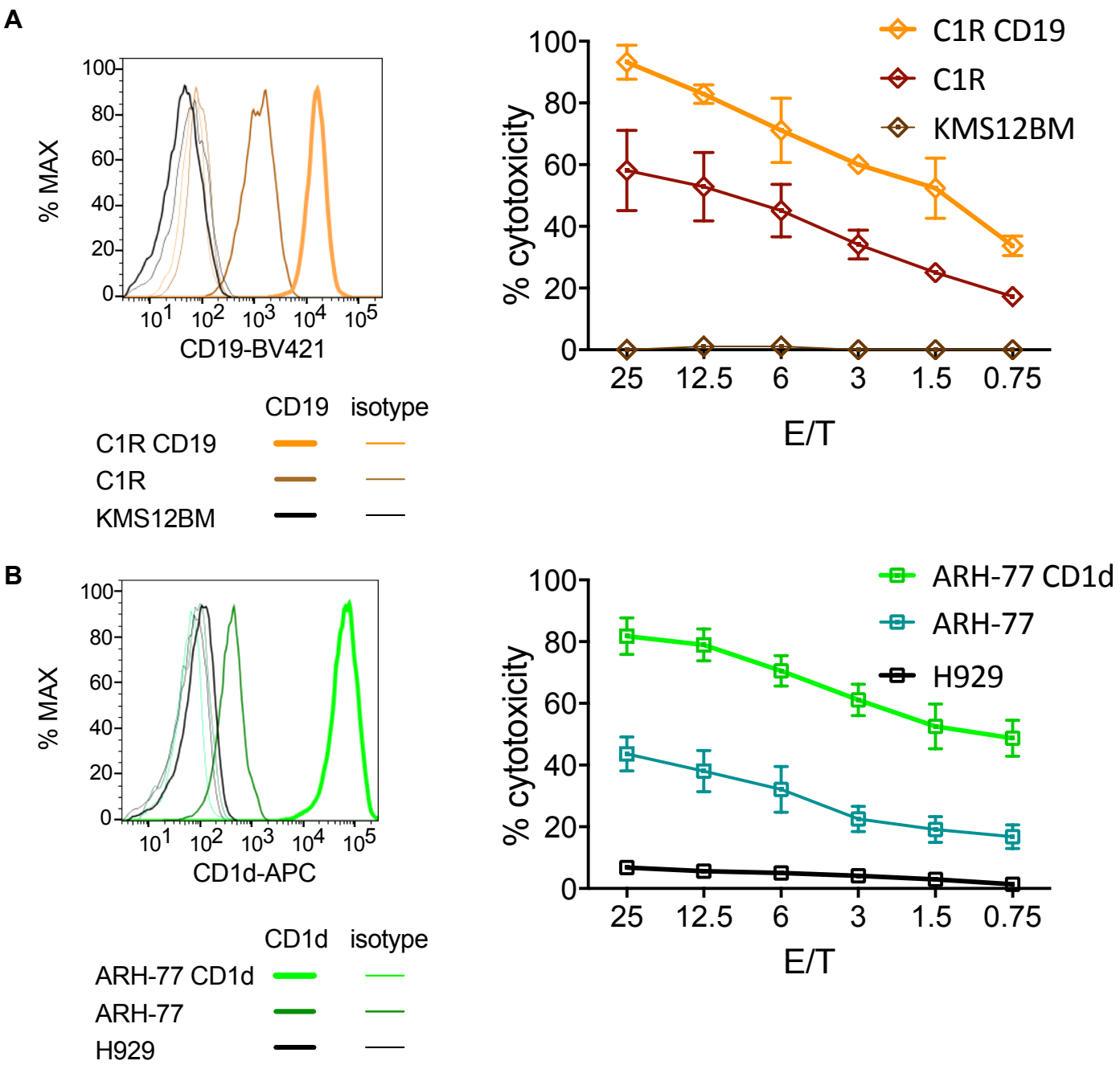

Figure S2 (Related to Figure 3)
(A) Cytotoxic activity of CAR19-iNKT cells (right) against C1R cells with high and low levels of CD19 expression (left). The B lineage myeloma cell line KMS12BM was used as a $CD19^-$ control.
(B) Cytotoxic activity of CAR19-iNKT cells (right) against ARH77 cells expressing low or high levels of exogenous CD1d (left); the B lineage myeloma cell line H929 was used as a $CD1d^-$ control.

Error bars represent SEM of triplicate assays.

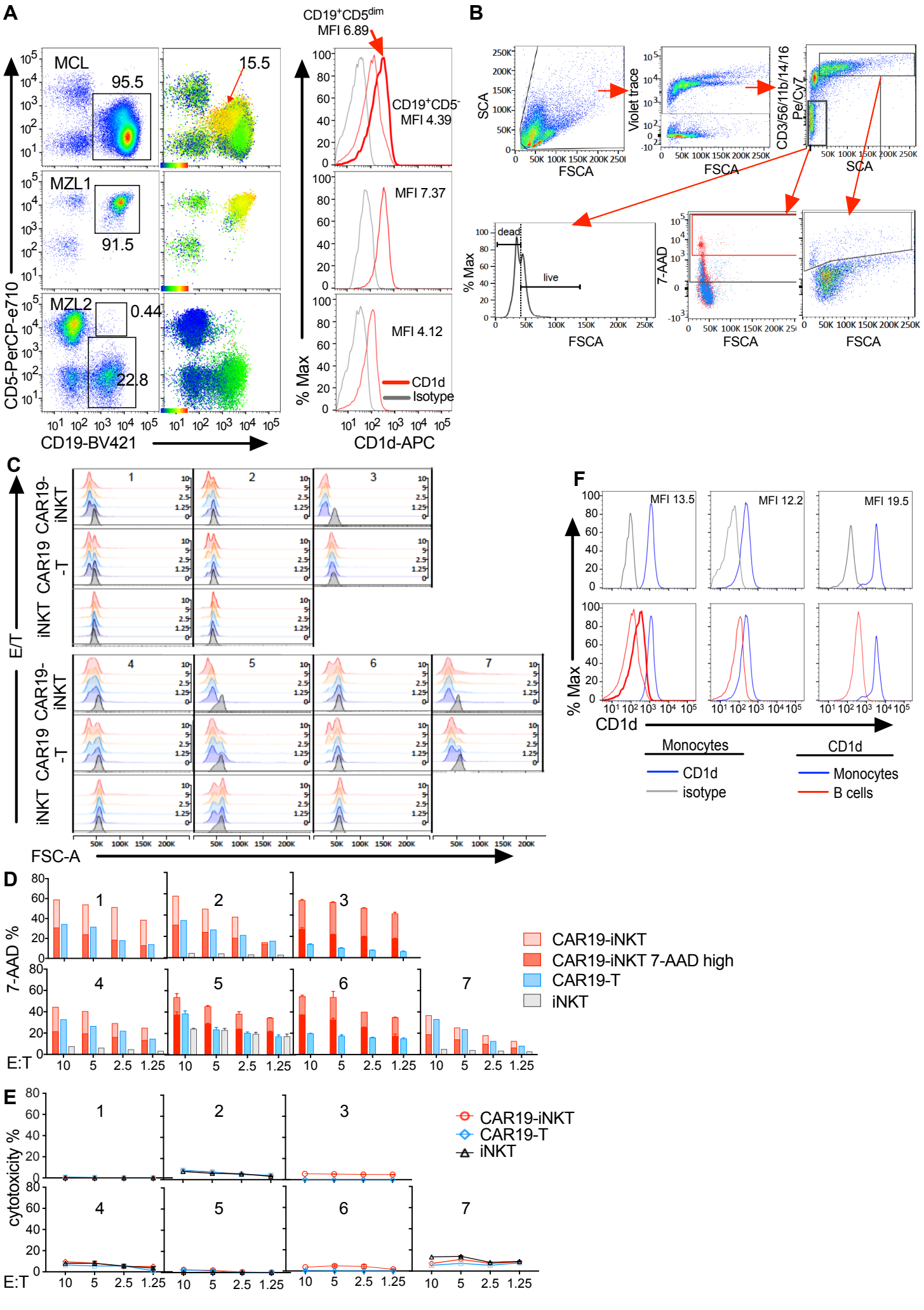
A
MCL
95.5
15.5
MZL1
91.5
MZL2
0.44
22.8
CD5-PerCP-e710
CD19-BV421
CD19+CD5dim
MFI 6.89
CD19+CD5-
MFI 4.39
MFI 7.37
MFI 4.12
CD1d
Isotype
% Max
CD1d-APC
B
SCA
FSCA
Violet trace
CD3/56/11b/14/16
Pe/Cy7
dead
live
% Max
7-AAD
C
CAR19-iNKT
CAR19 -T
iNKT
E/T
FSC-A
D
7-AAD %
E:T
CAR19-iNKT
CAR19-iNKT 7-AAD high
CAR19-T
iNKT
E
cytotoxicity %
E:T
CAR19-iNKT
CAR19-T
iNKT
F
MFI 13.5
MFI 12.2
MFI 19.5
% Max
CD1d
Monocytes
CD1d
isotype
CD1d
Monocytes
B cells

Figure S3 (Related to Figure 3)
(A) Flow-cytometric analysis of CD19 and CD1d co-expression on peripheral blood lymphoma cells from one patient with blastic variant of MCL and two patients with MZL. Left: malignant cells are boxed; middle: expression of CD1d is shown as heat-map on the CD5/CD19 dot plots and is colored according to intensity of expression; right: expression of CD1d in the form of histograms. Note the presence of 2 different lymphoma populations with different levels of CD1d expression in the patient with MCL.
(B) Gating strategy of flow cytometric cytotoxicity assay for in 'the same tube' analysis of lymphoma cells (Violet^{+}, CD19^{+}CD3/56/11b/14/16^{-}, SCA^{low}) and monocytes (Violet^{+}, CD3/56/11b/14/16^{+}, SCA^{high}). Dead cells were identified as 7-AAD^{+} events, with high and intermediate 7-AAD intensity corresponding to necrotic and apoptotic cells respectively. Cell death was also assessed by cell size (FSC-A) with smaller cells corresponding to apoptotic/necrotic cells (see also methods).
(C) Flow cytometry histograms showing FSC-A-based cell size analysis of primary lymphoma target cells in cytotoxicity assays with CAR19-iNKT, CAR19-T and untransduced iNKT cells.
(D) Fractions of 7-AAD^{high} and 7-AAD^{dim} primary lymphoma cells in cytotoxicity assays with CAR19-iNKT, CAR19-T and untransduced iNKT cells.
(E) Cytotoxic activity of CAR19-iNKT, CAR19-T and untransduced iNKT cells against monocytes in assays shown in Figure 3F and Figure S3C-D.
(F) Flow cytometry histogram overlays showing CD1d expression in monocytes of patients shown in (A). Normalized MFI values (ratio between CD1d and isotype control MFIs) are shown.

Error bars represent SEM of triplicate assays

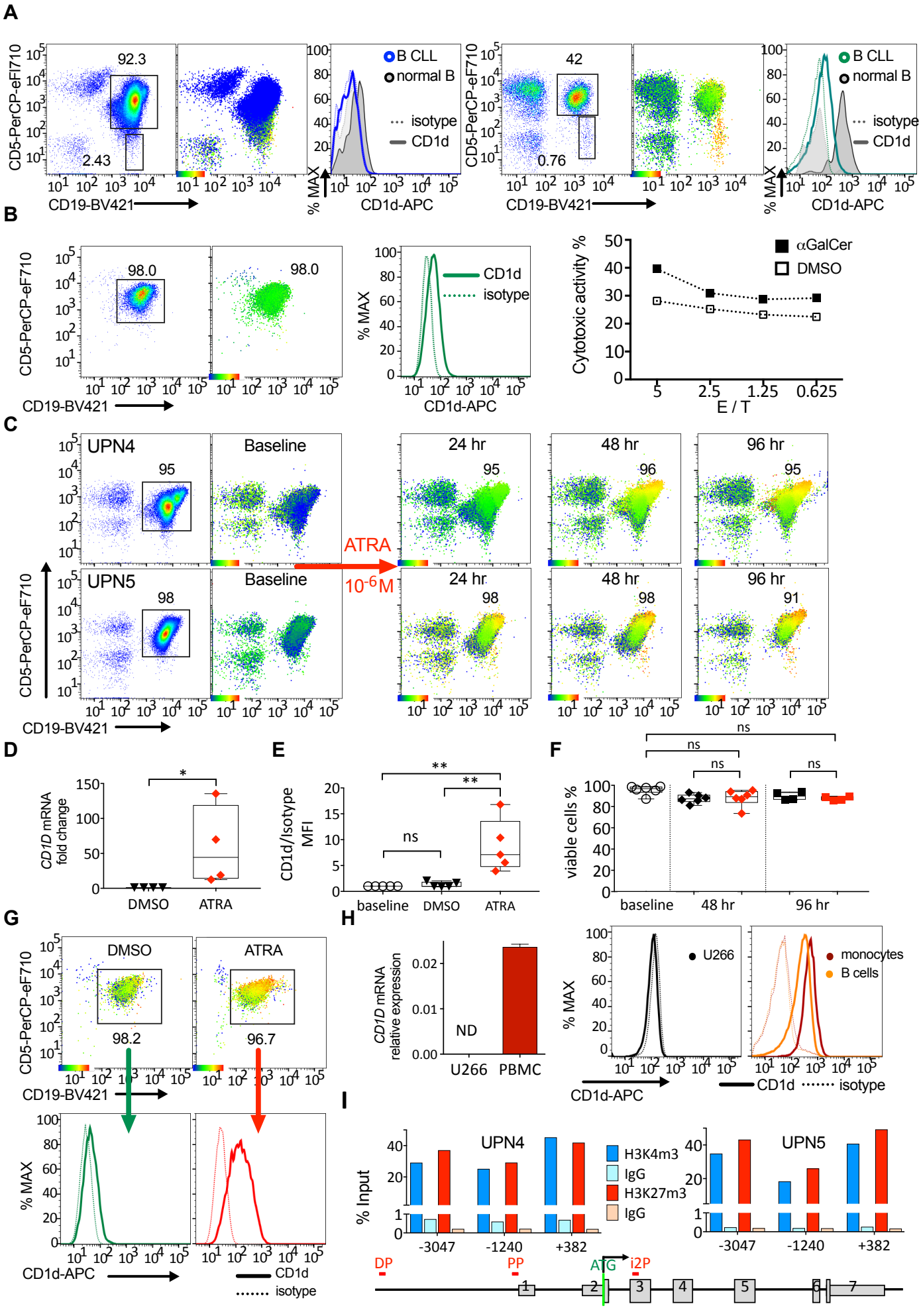
A
CD5-PerCP-eFl710
92.3
2.43
CD19-BV421
B CLL
normal B
isotype
CD1d
% MAX
CD1d-APC
42
0.76
B
CD5-PerCP-eF710
98.0
αGalCer
DMSO
Cytotoxic activity %
E / T
C
UPN4
UPN5
Baseline
24 hr
48 hr
96 hr
95
96
98
91
ATRA
10-6M
D
CD1D mRNA fold change
DMSO
ATRA
E
CD1d/Isotype MFI
baseline
F
viable cells %
ns
G
98.2
96.7
H
CD1D mRNA relative expression
ND
U266
PBMC
monocytes
B cells
I
UPN4
UPN5
% Input
H3K4m3
IgG
H3K27m3
-3047
-1240
+382
DP
PP
ATG
i2P

Figure S4 (Related to Figure 4)

(A) No or low CD1d expression in CLL cells from patients UPN1 and UPN2 in comparison to normal B cells. Peripheral blood CLL B cells are $CD19^{+}CD5^{+}$ while non-malignant B cells are $CD19^{+}CD5^{-}$. CD1d expression is shown as a heatmap on CD19/CD5 dot plots (middle) and as histogram overlays (right).

(B) Cytotoxic activity of 2nd generation CAR19-iNKT cells against CLL cells in the presence of DMSO control or αGalCer (right). Expression level of CD1d on CLL cells is also shown by heatmap on dot plot and histogram analysis (left). Error bars represent SEM of triplicate assays.

(C) Combined dot-plot/heatmap analysis of CD1d expression in CLL cells treated with 10^{-6} M ATRA for 0-96 hr.

(D) Relative increase of *CD1D* mRNA as assessed by qPCR expression on CLL cells treated with 0.1% DMSO or 10^{-6} M ATRA for 0 or 48 hr (n=4 patients).

(E) Relative increase of CD1d cell surface expression as assessed by CD1d/isotype ratio as described in D (n=5).

(F) No effect of ATRA on CLL cell viability as assessed by trypan blue staining. Horizontal line in box-whisker plots in (D-F) shows median and upper and lower horizontal lines of box represent 75th and 25th percentile respectively and whiskers represent 95th and 5th percentiles.

(G) Combined dot-plot/heatmap analysis of CD1d expression in CLL cells treated with 0.1% DMSO or 10^{-6} M ATRA for 48 hr and subsequently used to test 2nd and 3rd generation CAR19 effector reactivity in the cytotoxicity assay shown in Figure 4D.

(H) CD1d expression in U266 compared to peripheral blood mononuclear cells from healthy individuals. Left: relative mRNA levels as assessed by qPCR (n=3); right: representative flow cytometric histograms showing CD1d mean fluorescent intensity (MFI) in U266 cells compared to normal blood B cells and monocytes relative to isotype controls. ND: not detected. Error bars are SEM.

(I) ChIP-qPCR assay showing bivalent histone state of *CD1D* in primary CLL cells from the same two patients shown in Figures 4A-C and Fig S4C. There is relative enrichment for H3K4m3 and H3K27m3 marks in relation to Ig control. The 3qPCR amplicons spanning the 5' UTR (DP: distal; PP: proximal, relative to the ATG start codon) and the gene body (i2P: within exon 2) of *CD1D* are shown. Representative of 2 independent experiments.

*: $p<0.05$; **: $p<0.01$; ns: not significant

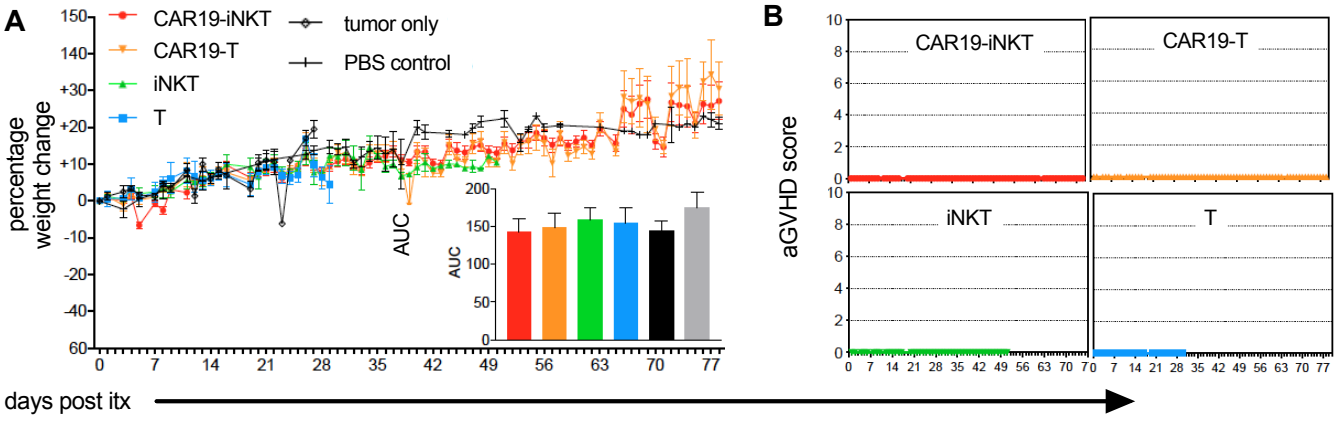
A
CAR19-iNKT
CAR19-T
iNKT
T
tumor only
PBS control
percentage weight change
AUC
days post itx
B
CAR19-iNKT
CAR19-T
iNKT
T
aGVHD score

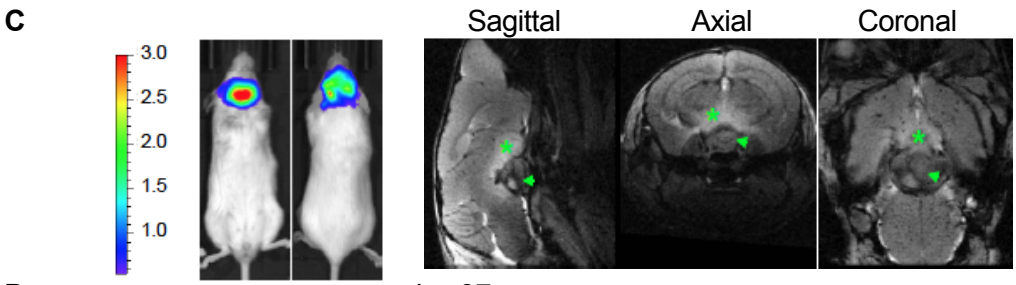
C
Sagittal
Axial
Coronal

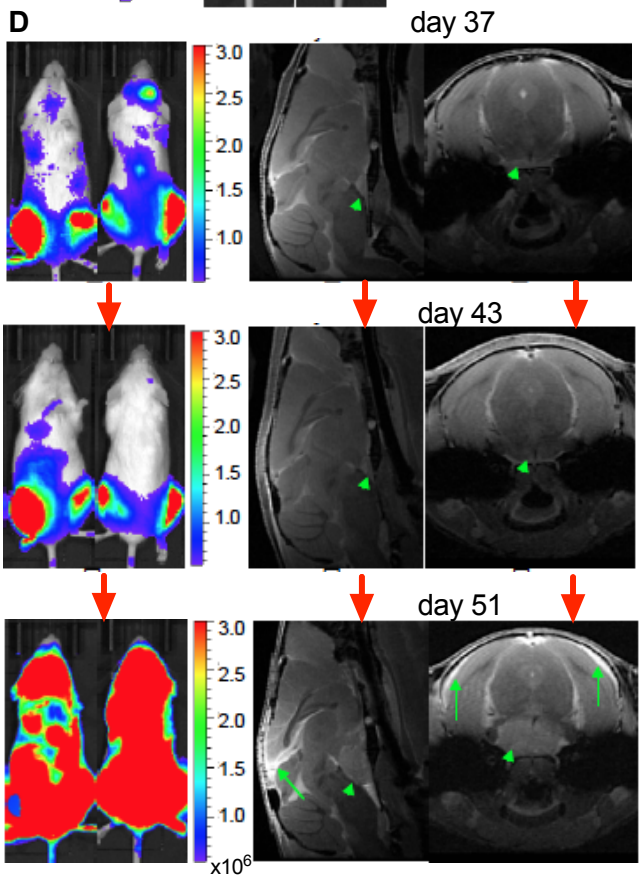
D
day 37
day 43
day 51
x10^6

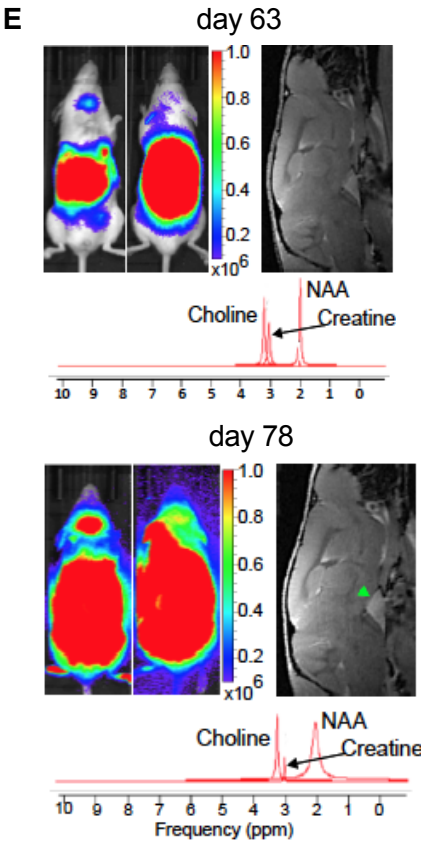
E
day 63
day 78
Choline
NAA
Creatine
Frequency (ppm)

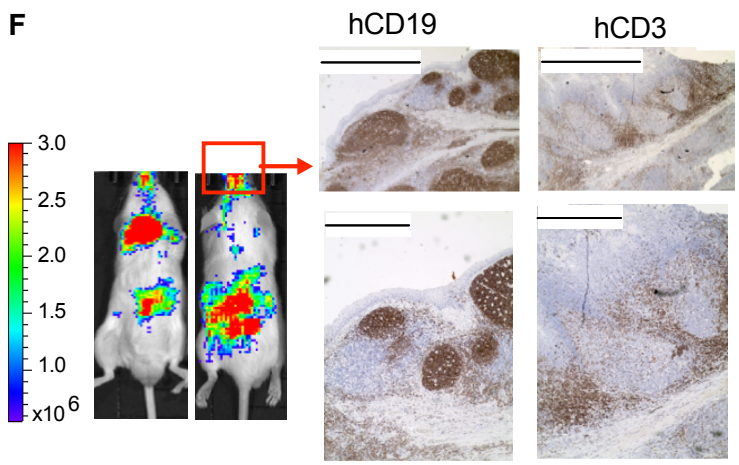
F
hCD19
hCD3
x10^6

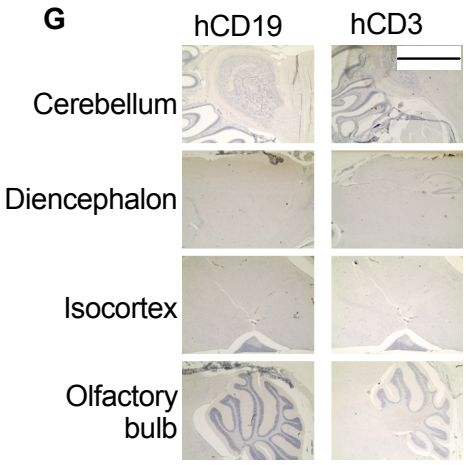
G
hCD19
hCD3
Cerebellum
Diencephalon
Isocortex
Olfactory bulb

Figure S5 (Related to Figures 5 and 6)

(A) Relative body weight change in all experimental groups shown as mean ± SEM. Area under the curve (AUC) was calculated until day 27 when there was at least 1 animal alive per group.

(B) aGVHD score, on a scale of 0-10, was 0 in all groups.

(C) Correlation of BLI signal with brain MRI study in a CAR19-T cell-treated animal. Left: BLI images obtained on day +21 post immunotherapy. Right: representative mouse (m) sagittal, axial and coronal MRI sections obtained on day +23 post immunotherapy after contrast injection (Gadovist 3mmol/kg iv) and acquired with T1 FLASH sequence to maximize the Gadolinium signal. The terminal MRI study showed a sellar mass (arrow heads) of 21.4 mm^3 (± 0.2) and suprasellar parenchymal enhancement (asterisks), suggestive of lymphomatous growth in the pituitary gland and in the parenchymal tissue.

(D) Correlation of BLI images with brain MRI study in an iNKT cell-treated animal. The animal stopped gaining weight from day +36 post-immunotherapy. Longitudinal MRI study showed a steadily growing mass in the pituitary region (arrow heads), with an estimated volume of 4.72 mm^3, 7.79 mm^3 and 28.2 mm^3 on day +37 (top), +43 (middle) and +51 (bottom) respectively. Eventually, the mouse became hypoactive, which was associated with the appearance of diffuse, smooth extra-axial contrast enhancement along the cerebral convexity bilaterally, suggestive of meningeal infiltration by tumor cells (long arrows).

(E) Correlation of BLI images with MR spectroscopy (MRS). Longitudinal MRI and MRS study in a CAR-T cell treated animal. Top: MRS assessment on day+63 post-immunotherapy underpinned low burden head disease, which upon MR spectroscopic analysis was characterized by inversion of the Choline/Creatine (frequency: 3.2/3.0) and Choline/NAA (frequency: 3.2/2.0) peaks at LTE compared to normal control (**Table S1**). Bottom: Head disease progression was confirmed by BLI, MRI and MRS on day +78, showing increased bioluminescence signal from the head, enlarged sellar mass (from 6.382mm^3 ± 0.235 to 7.429 ± 0.033, arrow heads) and elevated Choline/Creatine and Choline/NAA ratios. MRS data are shown as chemical shifts expressed in parts per million (ppm) relative to the reference Tetramethylsilane (TMS, frequency 0.00 ppm).

(F) Representative BLI images and immunohistochemistry. Left: BLI evidence of brain disease of a mouse treated with CAR19-T cells and died on day 27. Right: staining with anti-human CD19 (hCD19) and CD3 (hCD3) of the same animal olfactory bulb brain tissue. The tumor cells were identified by bright CD19 staining, whereas CAR19-T cells were revealed by $CD3^+$ staining at the edge of the tumor areas. Top microphotographs scale bar: 500 μm; bottom microphotographs scale bar: 200 μm.

(G) The same immunohistochemical analysis on day 90 (i.e., end of the *in vivo* experiment) was performed on CAR19-iNKT cell-treated animals. Representative example is from an animal that achieved second remission shown in Figure 6C. No $CD19^+$ or $CD3^+$ cells were detected. Scale bar for all microphotographs: 1 mm.

A

Chemokine	Chemokine Receptor	Chemokine	Chemokine Receptor
CCL2	CCR2	CCL16	CCR1, CCR2
CCL3	CCR5, CCR1, CCR4	CCL17	CCR4
CCL4	CCR5	CCL20	CCR6
CCL5	CCR1, CCR3, CCR5	CCL22	CCR4
CCL7	CCR1, CCR2, CCR3	CCL25	CCR9
CCL12	CCR2	CXCL10	CXCR3
CCL13	CCR2, CCR3	CXCL16	CXCR6

Modified from IUIS/WHO Subcommittee on Chemokine Nomenclature, 2003

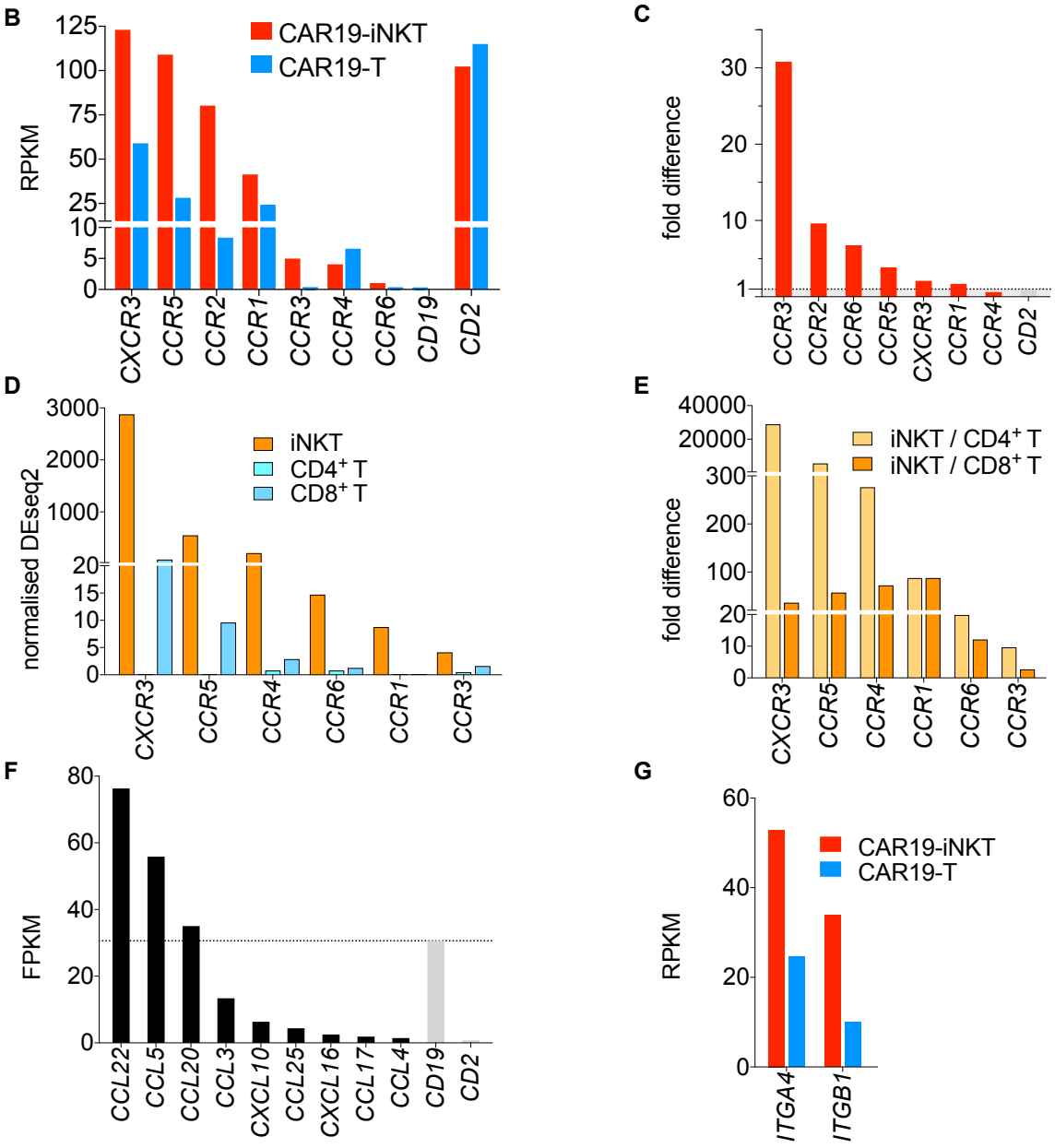

Figure S6 (Related to Figure 6)

(A) Chemokines and their receptors as per IUIS/WHO Subcommittee on Chemokine Nomenclature, 2003 (IUIS/WHO, 2003).

(B and C) Chemokine receptor mRNA expression as assessed by RNA-seq in CAR19-iNKT and -T cells shown as RPKM (B) and fold-difference of CAR19-iNKT over CAR19-T cells (C). Expression values of *CD2* and *CD19* and fold difference of *CD2* mRNA are shown as reference.

(D and E) Chemokine receptor mRNA expression in murine splenic iNKT $CD4^+$ and $CD8^+$ T cells (D) and fold-difference (E). Data mined from Skyline (RNA-seq) at http://www.immgen.org/.

(F**)** CCL and CXCL family chemokine mRNA expression (shown as FPKM) in C1R-CD1d parental lymphoma cells as assessed by RNA-seq. *CD2* and *CD19* mRNA expression values are shown as reference.

(G**)** *ITGA4* and *ITGB1* mRNA expression as assessed by RNA-seq in CAR19-iNKT and -T cells (shown as RPKM).